Isomer Populations in Liquids for 1-Isopropyl-3-methylimidazolium Bromide and Its Iodide and Their Conformational Changes Accompanying the Crystallizing and Melting Processes

Takatsugu Endo[†] **and Keiko Nishikawa***[,‡]

Graduate School of Science and Technology, Chiba University, 1-33 Yayoi-cho, Inage-ku, Chiba 263-8522, Japan, and Graduate School of Advanced Integration Science, Chiba University, 1-33 Yayoi-cho, Inage-ku, Chiba 263-8522, Japan

Received: April 14, 2008; Revised Manuscript Received: May 28, 2008

Most ionic liquids (ILs) are characterized by the presence of some kind of isomer for component ions. We investigated the liquid and crystalline structures of 1-isopropyl-3-methylimidazolium halides ([*i*-C_3mim]X, X = Br, I) by means of Raman scattering measurements backed up by density functional theory (DFT) calculations. The DFT calculations indicated that there are two stable rotational isomers of [*i*-C_3mim]$^+$, one of an asymmetric form (**Asym**) and the other a symmetric one (**Sym**). For both salts, it was revealed that **Asym** and **Sym** coexist in liquid states, in contrast to the presence of only **Asym** in crystalline states. We determined the isomer populations and showed that **Asym** is dominant in the liquid states of both salts (approximately 7/3). Conformational changes in [*i*-C_3mim]$^+$ during the crystallizing and melting processes were observed by conducting simultaneous measurements using the techniques of Raman spectroscopy and calorimetry. We have revealed that the conformational change from **Asym** to **Sym** occurs gradually, with linking to melting in the premelting region. This is a conclusive observation of the structural changes of ILs in the premelting region and demonstrates the conformational changes between isomers during the crystallizing and melting processes.

1. Introduction

Ionic liquids (ILs) are a new class of compounds with a low melting temperature despite their being composed of solely ions. They have attracted much attention as functional liquids and green solvents due to their unique properties.[1–5] The uniqueness of ILs is particularly conspicuous in their thermal behaviors for example, low melting point, premelting over a wide temperature range, excessive supercooling, tendency toward glass formation from the liquid state upon cooling, and extreme thermal history. The relationship between these features and structures of constituent ions has been recently identified.[6–12] For example, Holbrey et al.[8] reported on the crystalline polymorphs of 1-butyl-3-methylimidazolium ([C_4mim]) chloride, and pointed out that the polymorph of ILs is one of the reasons for low melting temperature. Some papers have indicated that the degree of supercooling of imidazolium ILs strongly depends on the alkyl chain length of the cation.[9–11]

We have shown the complex crystallizing behavior and unique premelting phenomenon of typical ILs, [C_4mim] halides, using a nW-stabilized differential scanning calorimeter (DSC).[12] It can be inferred that these characteristic behaviors were due to the cooperative conformational changes of the butyl group in [C_4mim]$^+$ linking to the melting and crystallizing processes. However, calorimetry does not provide information on exactly what the change is. Recently, through simultaneous measurements conducted using the techniques of Raman spectroscopy and calorimetry, we have directly observed the conformational change of the butyl group in [C_4mim]$^+$ linking to the melting in the premelting region.[13]

CHART 1: Structure and Atomic Numbering for the [*i*-C_3mim]$^+$ Ion

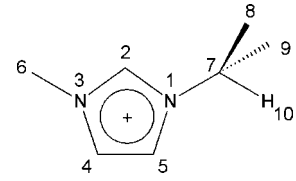

In this study, we chose 1-isopropyl-3-methylimidazolium halides ([*i*-C_3mim]X, X: Br and I; Chart 1) to determine the structure of the imidazolium cation in the liquid state and to conclusively investigate the conformational change of the alkyl group linking to phase transitions. Halide ions, as most simple anions, make it possible to focus on conformational analyses of the cation only. ILs including [*i*-C_3mim]$^+$ were predicted to have two stable rotational isomers in the gas phase by our preliminary theoretical calculation. This finding is similar to that for the 1-ethyl-3-methylimidazolium ion ([C_2mim]$^+$), which is the most popular and simple cation of ILs. As for [C_2mim]$^+$, the presence of two rotational isomers has been confirmed by both theoretical and experimental results.[14] Therefore, [*i*-C_3mim]X is suitable for observing the linking phenomenon. Since the isopropyl group in [*i*-C_3mim]$^+$ is more bulky than the ethyl group ([C_2mim]$^+$), it is expected that the alkyl group possesses some outstanding thermal properties and behaviors. There are few reports available on the structure of [*i*-C_3mim]$^+$-based ILs contrary to that of [C_2mim]$^+$, and there is no information on the liquid-state structure.

2. Experimental Section

2.1. Samples. [*i*-C_3mim]Br and [*i*-C_3mim]I were synthesized by the following procedure. A slightly excessive amount of

* To whom correspondence should be addressed. Phone: +81-43-290-3939. Fax: +81-43-290-3939. E-mail: k.nishikawa@faculty.chiba-u.jp.
† Graduate School of Science and Technology.
‡ Graduate School of Advanced Integration Science.

10.1021/jp8031989 CCC: $40.75
Published on Web 07/25/2008

individual isopropyl halide was added slowly to the THF solution of 1-methylimidazole and stirred in an Ar atmosphere. During this operation, the solution was cooled in an ice bath. The solution was then heated and refluxed overnight. The solvent was removed by rotary evaporation, and a yellow solid was obtained. The product was washed several times with ethyl acetate and recrystallized with acetonitrile/ethyl acetate to produce a colorless crystalline solid, which was dried under vacuum at room temperature for several hours. The obtained ILs were characterized by ^{1}H NMR (JEOL JNM-LA400). ^{1}H NMR (DMSO-d_6, δ/ppm relative to TMS): [*i*-C_3mim]Br 9.24 (s, 1H), 7.86 (s, 1H), 7.69 (s, 1H), 4.59 (m, 1H), 3.80 (s, 3H) 1.42 (d, 6H); [*i*-C_3mim]I 9.17 (s, 1H), 7.84 (s, 1H), 7.68 (s, 1H), 4.59 (m, 1H), 3.80 (s, 3H) 1.42 (d, 6H).

Because these ILs are hygroscopic, they were dried again under vacuum at 373 K for several hours before measurements were conducted. The water content of the ILs was <300 ppm as measured by Karl Fischer titration using a Mettler-Toledo model DL39 coulometer. For spectroscopic and calorimetric measurements, tens of milligrams of the individual sample were set in an aluminum vessel of a diameter of 6 mm and depth of 4 mm and sealed with a quartz plate using high-vacuum grease (Apiezon T) in an N_2 atmosphere glovebox to avoid absorption of atmospheric moisture. Both samples were in polycrystals.

2.2. Measurements. Using our developed apparatus,[13] we made measurements of Raman spectra at various temperatures and simultaneous measurements using Raman spectroscopy and calorimetry techniques focusing on the crystallizing and melting processes. The outline of the apparatus is as follows. The laboratory-made calorimeter is combined with the commercially available Raman spectrometer. The spectrometer is a fiber optically coupled Raman spectrometer (Hololab, Kaiser Optical Systems) equipped with a GaAlAs diode laser (wavelength: 785 nm). The optical resolution is 4 cm^{-1}, and a spectrum in the range of 100−3450 cm^{-1} can be measured at the same time. As for the calorimeter, thermoelectric modules are used as both a heat flux sensor (9500/018/012, Ferro Tec) and a heat pump (6320/157/085, Ferro Tec). A free piston stirring cooler (TB40-SN8SG, Shinyei) is applied to obtain low temperatures down to 153 K. The temperature is measured using a Pt resistance thermometer (EL-700-U, Teijin Engineering). The baseline stability of the calorimetry trace is measured to be 5 μW. One of the characteristics of the calorimeter is the capability of carrying out heating and/or cooling experiments at an extremely slow rate sufficient for mimicking a quasi-static condition. From the standpoint of Raman spectroscopy, this apparatus can be regarded as a sample holder by which spectra at various temperatures ranging from 153 to 403 K can be obtained under sufficient stabilized thermal conditions. From the standpoint of calorimetry, the apparatus gives us direct information on the structure change of the sample during accompanying thermal phenomena. The laser power was set at less than 10 mW for simultaneous measurements to observe the in situ thermal behavior of ILs.

2.3. DFT Calculations. Density functional theory (DFT) calculations were carried out using the Gaussian 03 program package.[15] Both full geometry optimizations and normal frequency analyses for [*i*-C_3mim]$^+$ were calculated in the gas phase using 6-311+G(d,p) basis sets according to Becke's three-parameter hybrid method[16] with LYP correlation (B3LYP).[17,18] All optimized structures were found to produce no imaginary frequencies, which ensures the presence of a minimum. A scaling factor was applied to neither the calculated frequency nor thermal properties in this study.

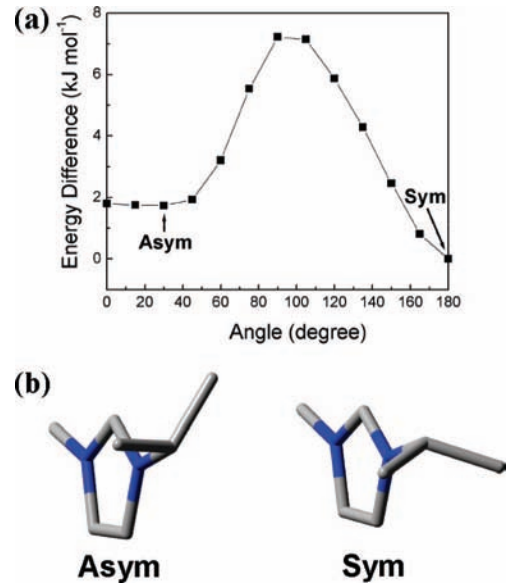

Figure 1. (a) Potential energies as a function of torsion angles for the C5−N1−C7−H10 of [*i*-C_3mim]$^+$. (b) Structures of two stable rotational isomers, **Asym** and **Sym**.

3. Results and Discussion

3.1. Potential Energy for Torsion Angle of [*i*-C_3mim]$^+$. First, it was indicated that the imidazolium ring forms a flat plane as the stable structure. We calculated the potential energy for the rotation of the isopropyl group of [*i*-C_3mim]$^+$ around the N1−C7 axis. The numbering for atoms is given in Chart 1. The dihedral angle of C5−N1−C7−H10 is defined as the torsion angle. Energy differences from the most stable one are shown in Figure 1a. Calculations indicated two local minima at torsion angles of ∼30 and 180°. These rotational isomers are shown in Figure 1b and are called the asymmetric form (**Asym**) and the symmetric form (**Sym**), respectively. Here, **Sym** refers to the arrangement where two methyl groups in the isopropyl group are positioned symmetrically against the imidazolium ring. As for **Asym**, the plane formed by N1−C7−C8 is almost perpendicular to the plane of the imidazolium ring. **Sym** is slightly more stable than **Asym**. The existence of the two stable isomers in the cation is the same in [C_2mim]$^+$,[14,19] but not in [C_3mim]$^+$ (there exist four stable isomers in the calculation results).[19] This implies that the behavior in the structural change by the rotation around the N1−C7 axis and followed properties of [*i*-C_3mim]$^+$ may be similar to [C_2mim]$^+$ rather than [C_3mim]$^+$.

It is noted that there are two characteristics of [*i*-C_3mim]$^+$ obtained from the calculation results. One is the higher activation energy barrier for rotational isomerization as compared to [C_2mim]$^+$. The barrier was calculated to be ∼5 kJ mol^{-1}, and that of [C_2mim]$^+$ was less than 1 kJ mol^{-1}.[14] The isomerization of [*i*-C_3mim]$^+$ would be more difficult than that for [C_2mim]$^+$. The second is that there is little energy difference between −40 and 40° of the torsion angle of the isopropyl group (energy difference is ∼0.1 kJ mol^{-1}). This means that there is the possibility of various rotational isomers existing with little rotation from **Asym**. Actually, Kawahata et al. have identified a unique crystal structure of [*i*-C_3mim]Br that consists of three independent rotational isomers of the cation.[20] The torsion angles of these cations are slightly different from those of **Asym**. However, we can safely classify them all as being **Asym**. Easy rotation of the isopropyl group in **Asym** is responsible for this unique crystal structure.

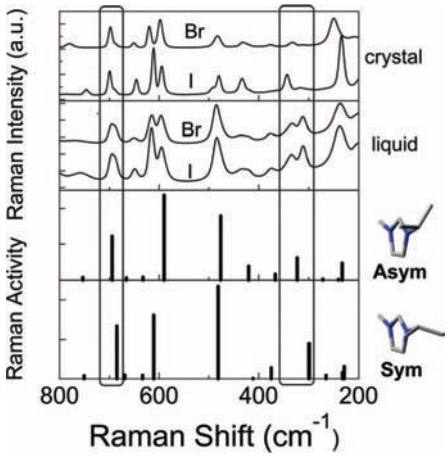

Figure 2. Observed Raman spectra of Br and I salts in their crystalline states at room temperature (above), liquid states at 393 K (middle), and calculated Raman bands of **Asym** and **Sym** (below). The bands enclosed by boxes are the marker bands for **Asym** and **Sym**.

TABLE 1: Calculated Raman Bands for Two Rotational Isomers of the [*i*-C$_3$mim]$^+$ Ion, Dipole Moments for Each Isomer, and Differences of Thermodynamic Variables (Asym − Sym)

	Asym		**Sym**	
	ν_{cal} (cm^{-1})	I_{Raman} (Å^4 amu^{-1})	ν_{cal} (cm^{-1})	I_{Raman} (Å^4 amu^{-1})
	233.0	0.93	228.9	0.63
	240.5	0.04	232.4	0.32
	271.8	0.06	265.5	0.18
	322.4	1.23	298.9	1.80
	366.6	0.34	374.9	0.56
	420.1	0.79	411.3	0.02
	476.2	3.59	481.3	4.69
	589.8	4.72	610.9	3.23
	632.4	0.17	633.3	0.18
	665.9	0.13	669.1	0.20
	694.4	2.44	685.0	2.67
	753.2	0.15	750.6	0.16
dipole moment (*D*)	2.26		2.68	
ΔE_0 (kJ mol^{-1})	1.6			
ΔH (kJ mol^{-1})	1.7			
ΔS (J K^{-1} mol^{-1})	5.9			
ΔG (kJ mol^{-1})	−0.5			

Golovanov et al. have reported a different crystal structure for [*i*-C$_3$mim]Br[21] from that of Kawahata,[20] which indicates that [*i*-C$_3$mim]Br has crystal polymorphism. The cation conformation reported by Golovanov et al. is **Sym**. On the contrary, only one crystal structure is reported for [*i*-C$_3$mim]I, and the cation conformation is **Asym**.[22]

3.2. Observed and Calculated Raman Spectra. We have investigated the conformations in the crystal and liquid states of both [*i*-C$_3$mim]Br and [*i*-C$_3$mim]I using the Raman spectroscopy technique and DFT calculations. The observed and calculated Raman bands are shown in Figure 2 and listed in Table 1 in the range of 200−800 cm^{-1}. Table 1 also includes the calculation results of dipole moments and the differences of zero-point-corrected energies (ΔE_0), enthalpies (ΔH), entropies (ΔS), and Gibbs free energies (ΔG) between **Asym** and **Sym**. The difference values of these thermodynamic properties are used later. Raman spectra of [*i*-C$_3$mim]Br and [*i*-C$_3$mim]I in their crystalline state are similar to one another. Since halide anions have no vibrational mode, each Raman band in this region is attributed to the vibrational mode of the cation. Comparing observed and calculated Raman spectra, the observed bands at 332 and 698 cm^{-1} of [*i*-C$_3$mim]Br and at 343 and 699 cm^{-1} of [*i*-C$_3$mim]I correspond to the calculated bands at 322.4 and 694.4 cm^{-1} and are assigned to **Asym**. There are weak observed bands at 312 and 687 cm^{-1} of [*i*-C$_3$mim]Br and at 316 and 689 cm^{-1} of [*i*-C$_3$mim]I. They correspond to calculated bands at 298.9 and 685.0 cm^{-1}, which are assigned to the **Sym** conformer. It is confirmed that the conformations of most of the cations in crystalline [*i*-C$_3$mim]Br and [*i*-C$_3$mim]I are **Asym** when it is synthesized and crystallized by the above-mentioned procedures. These results were reproducible for repeating the melting and crystallizing processes.

From the weak Raman bands, it is presumed that small amounts of **Sym** are included. As for the crystalline [*i*-C$_3$mim]Br, two causes are considered; one is the mixing of two isomorphs formed by **Asym** and **Sym**, and another is the mixing of the liquid on the surface and/or boundaries of **Asym** crystals. Since, as for the **Sym** crystal, the synthesis and crystallization procedures have not been presented in Golovanov's paper,[21] it is possible to know neither which isomorph is easy to crystallize nor to what degree the two isomorphs were mixed. We think that a small amount of **Sym** in the Raman spectrum is due to surface and/or boundary melting. Surface or boundary wetting are often observed in the crystals of ILs. We think that this is because the variety of conformations of component ions makes the ILs hard to crystallize, and portions, where some conformers coexist, are left without crystallization. Actually, although the crystal formed by only **Asym** is reported for the [*i*-C$_3$mim]I crystal,[22] very weak bands assigned to **Sym** are also observed in our Raman spectra.

These results imply that the [*i*-C$_3$mim]Br crystal structure, including **Asym**,[20] is more stable than the one including **Sym**.[21] This is considered to be due to the entropy effect. It should be noted that the observed Raman spectra of [*i*-C$_3$mim]Br is slightly different from that of [*i*-C$_3$mim]I. This result corresponds to the existence of different crystal structures between [*i*-C$_3$mim]Br and [*i*-C$_3$mim]I, although both conformations of the cation are **Asym**.[20,22]

In a liquid state, the observed Raman spectra of both [*i*-C$_3$mim]Br and [*i*-C$_3$mim]I are also similar to each other. The Raman band assigned to **Sym** was apparent in each IL, which indicates the coexistence of two conformers in the liquid state. The coexistence of conformers has already been reported on several imidazolium-based ILs, [C$_2$mim]$^+$,[14] [C$_4$mim]$^+$,[23,24] and 1-hexyl-3-methylimidazolium cation ([C$_6$mim]$^+$).[25] These reports showed that coexistence in the liquid state is a general phenomenon in imidazolium ILs, and the entropy increase induced by such coexistence will lead to the low melting temperature and easy glass formation of ILs. The same consideration is applicable to ILs such as [*i*-C$_3$mim]$^+$.

3.3. Temperature Dependence of Raman Spectra. Temperature dependences of the Raman spectra of ILs were measured to experimentally estimate the enthalpy difference between **Asym** and **Sym**. The experiments were carried out using the following procedures. First, each crystalline sample was heated up to 393 K, where each sample was perfectly melted, and the sample was then cooled down to 293 K. The Raman spectra were obtained every 20 K steps in the cooling process. Therefore, the samples were in the liquid or supercooled liquid state as shown later by the calorimetry curves (Figure 6). Figure 3 shows the Raman spectra of each IL around the assigned bands in the temperature range from 393 to 293 K (Raman spectra of [*i*-C$_3$mim]I at 293 K are

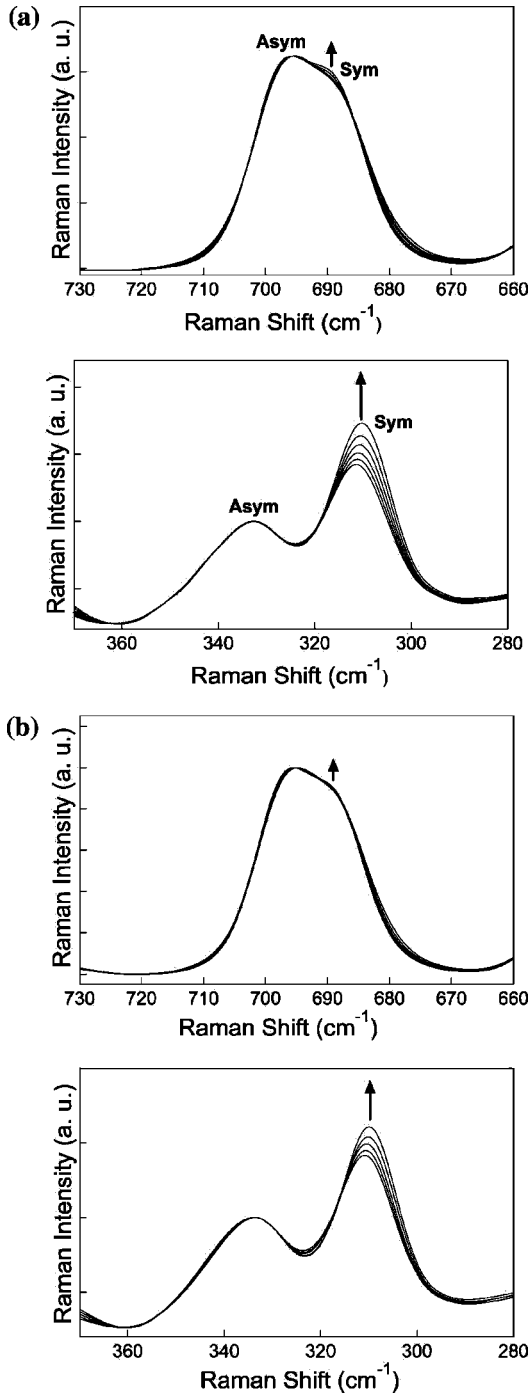

Figure 3. Temperature dependences of Raman spectra around the assigned bands. (a) Br salt in the temperature range of 393−293 K every 20 K steps. (b) I salt in the range of 393−313 K every 20 K steps. Arrows in the graphs indicate the experimental order from higher to lower temperature.

not shown because of crystallization). The Raman intensity was normalized to the **Asym** band intensity. With the decrease in temperature, all bands assigned to **Sym** showed an increase relative to the **Asym** bands, which indicates that **Sym** has more stability than **Asym** from the viewpoint of enthalpy.

To obtain the enthalpy difference between **Asym** and **Sym**, ΔH ($H_{\mathbf{Asym}} - H_{\mathbf{Sym}}$), the following three standard equations were used:

$$\Delta G = \Delta H - T\Delta S \tag{1}$$

$$\Delta G = -RT \ln \frac{u_{\mathbf{Asym}}}{u_{\mathbf{Sym}}} \tag{2}$$

and

$$\frac{u_{\mathbf{Asym}}}{u_{\mathbf{Sym}}} = \frac{m_{\mathbf{Sym}} I_{\mathbf{Asym}} \sigma_{\mathbf{Sym}}}{m_{\mathbf{Asym}} I_{\mathbf{Sym}} \sigma_{\mathbf{Asym}}} \tag{3}$$

where ΔG and ΔS are differences (**Asym** − **Sym**) of the Gibbs free energy and entropy and u is the molar fraction. The notation of m indicates conformational multiplicity, in this case $m_{\mathbf{Sym}}$ and $m_{\mathbf{Asym}}$ are 1 and 2, respectively. I is the integrated Raman band intensity, and σ is the Raman scattering cross section. From eqs 1, 2, and 3, we obtained the equation as follows:

$$-R \ln \frac{I_{\mathbf{Asym}}}{I_{\mathbf{Sym}}} = \Delta H \frac{1}{T} - \Delta S - R \ln \frac{m_{\mathbf{Asym}} \sigma_{\mathbf{Asym}}}{m_{\mathbf{Sym}} \sigma_{\mathbf{Sym}}} \tag{4}$$

The plot of $-R \ln(I_{\mathbf{Asym}}/I_{\mathbf{Sym}})$ against $1/T$ gives ΔH as the slope.

$I_{\mathbf{Asym}}$ and $I_{\mathbf{Sym}}$ were obtained by curve fitting of the assigned Raman bands. The curve fitting of the bands in the region of 290−360 cm^{-1} was difficult because there are at least three components and the region includes a nonlinear baseline. The bands in the region of 670−720 cm^{-1} were then fitted with two components of the mixed Gaussian and Lorentzian profile using Grams/AI software (Thermo Galactic). As an example, the fitting result for [*i*-C_3mim]Br at 393 K is shown in Figure 4a. The plot of $-R \ln(I_{\mathbf{Asym}}/I_{\mathbf{Sym}})$ as a function of $1/T$ is shown in Figure 4b. ΔH_{Br} for [*i*-C_3mim]Br and ΔH_{I} for [*i*-C_3mim]I are

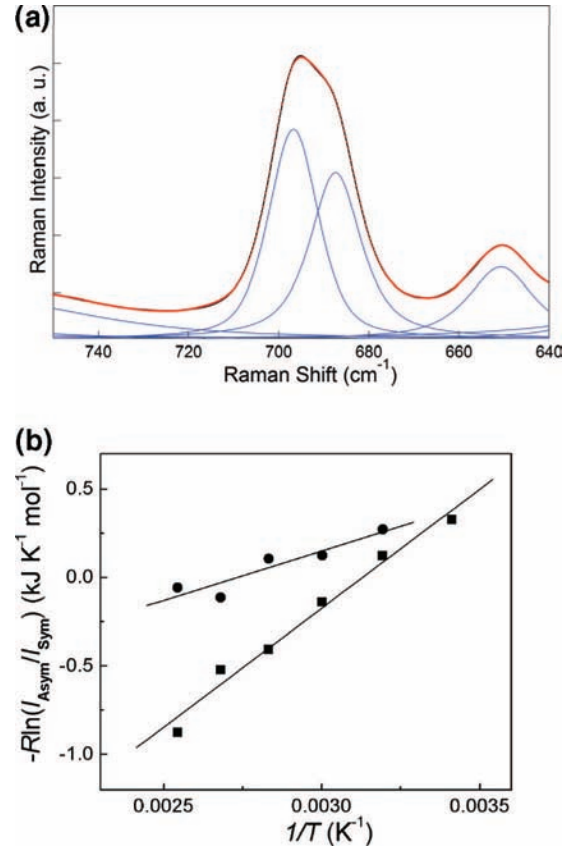

Figure 4. (a) Curve fitting profile of Raman bands of [*i*-C_3mim]Br at 393 K. Red dots indicate observed Raman bands, blue solid lines show separated spectral bands, and black solid line is sum of the separated bands. (b) Plots of $-R \ln(I_{\mathbf{Asym}}/I_{\mathbf{Sym}})$ as a function of $1/T$. Closed squares and circles are for Br and I salts, respectively.

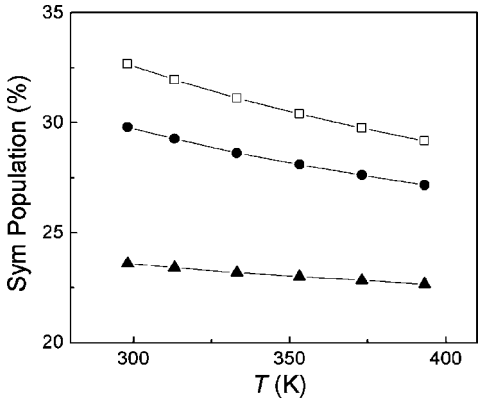

Figure 5. **Sym** populations at various temperatures. Open squares indicate [*i*-C_3mim]$^+$ using the results of the DFT calculation. Closed circles and triangles indicate Br and I salts, respectively, using the experimental results for the value of ΔH.

determined to be 1.3 and 0.6 kJ mol^{-1}, respectively. The result shows that **Sym** is slightly more stable than **Asym** in enthalpy. These values agree with the calculation of 1.7 kJ mol^{-1}. An agreement between experimental and calculated ΔH for isomerization has also been found for ILs, including [C_2mim]$^+$ [14] and bis(trifluoromethanesulfonyl) imide anion (Tf_2N^-).[26]

Note that **Asym** is slightly more stable than **Sym** in the calculation for Gibbs free energy, unlike that for enthalpy. This is attributed to the entropy effect, particularly vibrational entropy. The fact that **Asym** has higher entropy than **Sym** is considered reasonable, taking into account the easy rotation of the isopropyl group in **Asym**.

3.4. Estimation of Isomer Population. We can now estimate the isomer populations in the liquid states at various temperatures. In this study, two calculations were carried out for the estimation. Case 1 was conducted using eq 2 with only calculated parameters. Berg et al. reported on the population of two isomers in [C_6mim]$^+$ using this method.[25] They have indicated that the population of one conformer, which at 0.181 kJ mol^{-1} is more stable than another one in Gibbs free energy, is 52%. The populations of **Asym** and **Sym** in the present [*i*-C_3mim]$^+$ at 393 K are estimated to be 71 and 29%, respectively, by taking into account conformational multiplicity. The multiplicity effect on the population is more dominant than the difference of Gibbs free energy in [*i*-C_3mim]$^+$.

Although Case 1 is convenient, the fault with this method is that it does not include experimental factors and that its result is independent of the counteranion. Case 2, which includes experimental factors, uses the following equation derived from eqs 1 and 2 with multiplicity as

$$\frac{u_{\mathrm{Asym}}}{u_{\mathrm{Sym}}} = \frac{m_{\mathrm{Asym}}}{m_{\mathrm{Sym}}} \exp\left(\frac{\Delta S}{R} - \frac{\Delta H}{RT}\right) \qquad (5)$$

Calculated ΔS and observed ΔH were applied. A similar procedure has already been reported on the isomers in [C_2mim]$^+$ and in Tf_2N^-.[27] In the case of [*i*-C_3mim]$^+$, taking multiplicity into account, **Sym** populations at 393 K in Br and I salts are estimated to be 27 and 23%, respectively. These values including the experimental factor are similar to the value obtained from DFT calculations (29%). It should be noted here that these values also depend on the calculation method used. Different calculation methods or calculation levels will give different populations of isomers.

Sym populations obtained by the two procedures are plotted in Figure 5at various temperatures. The ratio of **Asym/Sym** is

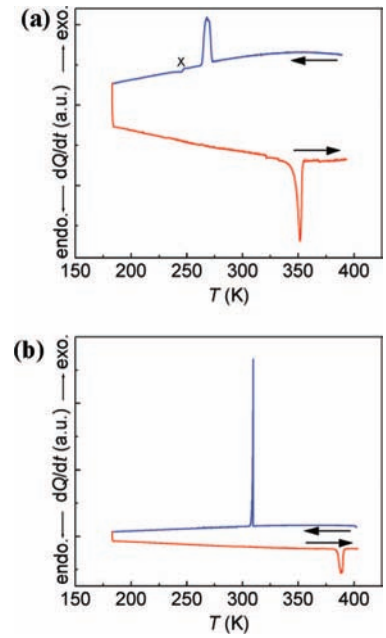

Figure 6. Calorimetry curves for (a) [*i*-C_3mim]Br and (b) [*i*-C_3mim]I at the scanning rate of 20 mK/s. Blue and red lines indicate the cooling and heating processes, respectively. The step denoted by "x" is the noise that is specific to this calorimeter.

within 72/28 (±5%) in the temperature range, independent of Br and I salts, and the population of **Asym** is significantly larger than that of **Sym**. The results can explain the wider supercooling range of [*i*-C_3mim]$^+$-based ILs than that of [C_2mim]$^+$. The supercooling ranges of [*i*-C_3mim]Br and [*i*-C_3mim]I are 84 and 79 K, respectively (described later), and those of [C_2mim]Br and [C_2mim]I are 49 and 40 K, respectively.[11] The supercooling of [*i*-C_3mim]$^+$ halides is clearly larger than that of [C_2mim]$^+$ halides despite the fact that the number of rotational isomers of the cation is the same. One reason for this would be the greater parity of the isomer populations for [*i*-C_3mim]$^+$ (72/28) than that for [C_2mim]$^+$ (87/13, ± 4%[27]); thus, the former is harder to crystallize. Note that a wider supercooling range of [*i*-C_3mim] halides will be also caused by the higher activation energy barrier for isomerization.

3.5. Conformational Changes during the Crystallizing and Melting Processes. The conformations of imidazolium-based ILs have been widely reviewed in both their crystalline and liquid states.[28] These studies indicate the conformational differences between their crystalline and liquid states.[14,24,28] It is also suggested that [C_4mim] halides melt accompanied by conformational changes in the premelting region.[12] However, to the best of our knowledge, there are no reports on the direct observation of the structural behavior during the change between the crystalline and liquid states except for our study on [C_4mim]Br.[13] Investigation of conformational changes during phase transitions will provide us with important information for understanding the characteristic thermal properties and behaviors of ILs.

Figure 6a and b shows calorimetry data of [*i*-C_3mim]Br and [*i*-C_3mim]I, respectively. The sample was heated up above the melting temperature to start the measurement from the liquid state so as to avoid imperfect thermal contact between the sample and the vessel. The sample in the liquid state was cooled at a rate of 20 mK/s to 183 K and once again heated at the same rate to above the melting temperature. Each trace had two peaks, an exothermic one upon cooling and an endothermic one upon heating, which correspond to the crystallizing and melting

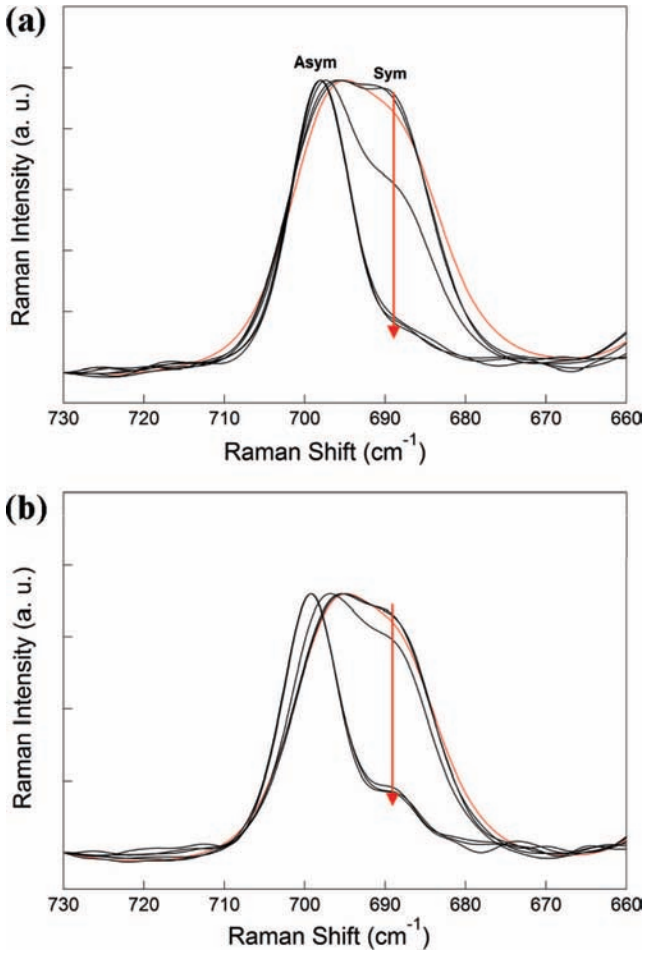

Figure 7. Raman spectra changes during the crystallizing process. (a) [*i*-C_3mim]Br spectra at temperatures from 280.9 to 279.9 K every 0.2 K steps. (b) [*i*-C_3mim]I spectra from 307.9 to 306.9 K every 0.2 K steps. For comparison, the spectra in liquid states at 393 K are shown by red curves.

processes, respectively. Both ILs showed a wide supercooling range, 84 K for [*i*-C_3mim]Br and 79 K for [*i*-C_3mim]I. These features indicate that [*i*-C_3mim] halides have the typical properties of ILs.

For investigation of conformational changes during the crystallizing and melting processes, we carried out simultaneous measurements using Raman spectroscopy and calorimetry techniques. The scanning rate of the calorimeter was 2 mK/s, and each Raman spectrum was collected every 100s (0.2 K/spectrum). Raman spectrum changes of the samples during the crystallizing process are shown in Figure 7a and b. The Raman intensity was normalized to the **Asym** band intensity. The behaviors are simple and similar in the bromide and iodide salts. The **Sym** band observed in the liquid state disappeared abruptly in the crystalline state via one medium spectrum for each of the salts. Melting behaviors of both samples were also similar to each other, as shown in Figure 8a and b. However, the melting behavior showed differences during the crystallizing process. **Sym** bands started to appear below the melting point and gradually increased in the premelting region with the rise in temperature. These results indicate that conformational changes are linked to melting in a manner similar to that for [C_4mim]Br.[13] In this measurement, the heating rate of 2 mK/s is slow enough to mimic the quasi-static process. Therefore, the premelting state could be considered as being a metastable phase including crystalline and liquid states with some rotational isomers.

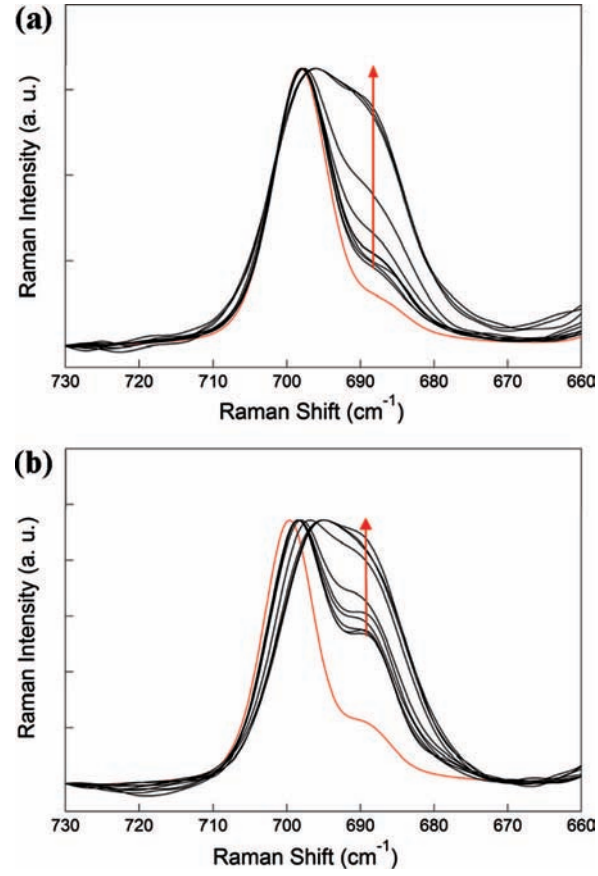

Figure 8. Raman spectra changes during the melting process. (a) [*i*-C_3mim]Br spectrum at temperatures from 351.1 to 352.9 K every 0.2 K steps. (b) [*i*-C_3mim]I from 385.6 to 387.4 K every 0.2 K steps. Red curves are the spectra in a crystalline state at room temperature.

To investigate the conformational changes during the crystallizing and melting processes in detail, changes in isomer populations during phase transitions were estimated by separating Raman bands into **Sym** and **Asym** components. The experimental values for ΔH were applied for this estimation. Raman spectra were normalized by an integrated Raman band intensity at a high wavenumber (2230−3360 cm^{-1}). **Sym** population changes and corresponding calorimetry curves for the crystallizing and melting processes are shown in Figures 9 and 10, respectively. The peak position for crystallizing in each calorimetry curve differs from that indicated in Figure 6. This is attributed to the difference of cooling rate. During the crystallizing process (Figure 9a and b), **Sym** populations of both samples were reduced instantaneously with a decrease in temperature, which corresponds to the calorimetry curves. A few **Sym** components for each sample, below 10%, remain in the crystalline state, which means that these samples are mixed crystals or may contain a liquid portion due to surface melting and/or boundary melting. During the melting process (Figure 10a and b), **Sym** populations of both samples below the melting temperature are shown to be larger than those in the case of the crystallizing process. **Sym** populations also show a gradual increase with the rise in temperature, corresponding to the calorimetry curves.

As shown in Figure 10b, two unique findings for [*i*-C_3mim]I were obtained from the simultaneous measurements. The first is that there is a higher **Sym** population in the premelting region (∼15%) compared to that for [*i*-C_3mim]Br (∼8%). This may be due to the looser interaction between the cation and the iodine ion as compared to the [*i*-C_3mim]Br case. Looser interaction

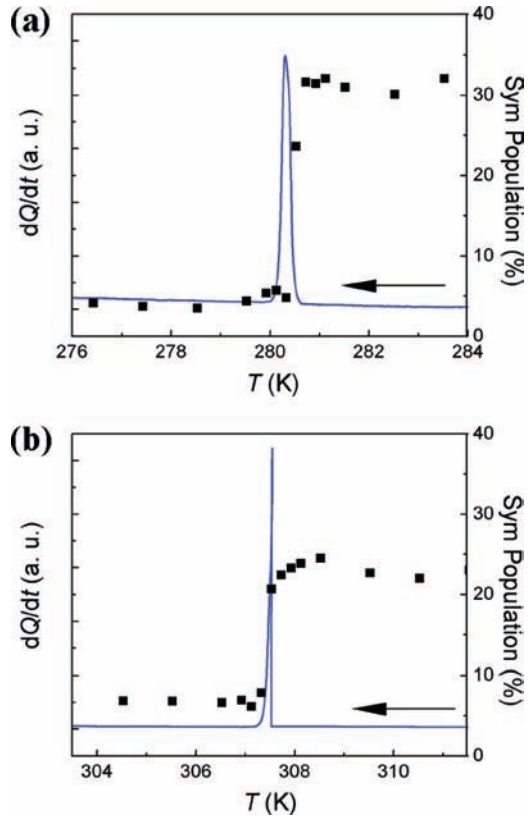

Figure 9. **Sym** populations and corresponding calorimetry curves during the crystallizing process. (a) [*i*-C_3mim]Br. (b) [*i*-C_3mim]I.

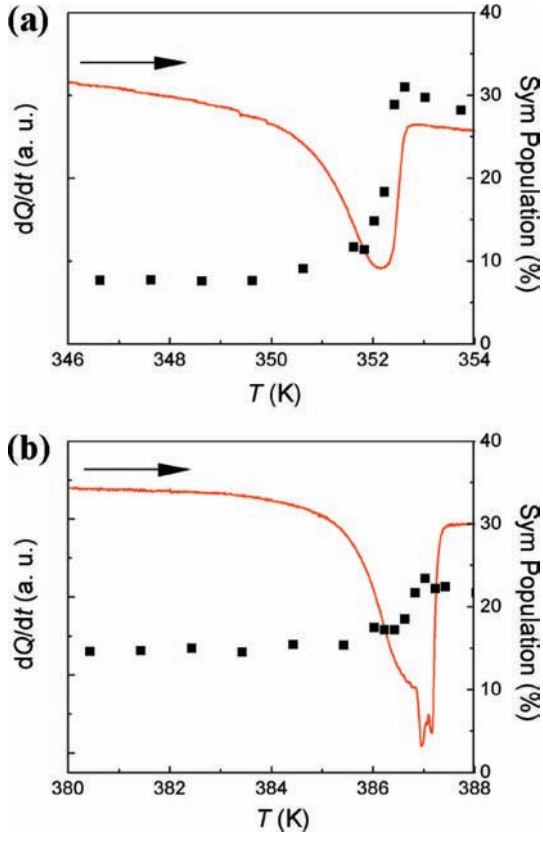

Figure 10. **Sym** populations and corresponding calorimetry curves during the melting process. (a) [*i*-C_3mim]Br. (b) [*i*-C_3mim]I.

enables easy conformational change between **Asym** and **Sym**. As for [*i*-C_3mim]I, values show a gradual increase from the point just after crystallization (~7%) to the starting point of melting (~15%). This shows that conformational change easily occurs even in a crystalline state. It is surprising that the value for the starting point of melting reaches 0.7 times the value for the liquid (~22%). The second is the multiple peaks on the calorimetric curve during melting. These peaks might be attributed to contamination of the sample or laser perturbation for Raman measurements. However, we consider these peaks to be intrinsic to [*i*-C_3mim]I because the measured sample was of a high level of purity (colorless crystalline solids and water content < 300 ppm), and multiple peaks were also observed on the calorimetric measurements without laser perturbation. Experiments are currently underway to interpret this phenomenon.

In conclusion, we have definitely and directly observed the conformational change of [*i*-C_3mim]$^+$ linking to the crystallizing and melting processes. Moreover, we have obtained information on structural behaviors in the premelting region, which is an equilibrium state distinguished from liquid and crystalline states.

4. Conclusion

Structures in the liquid and crystalline states of the [*i*-C_3mim]$^+$ ion and structural changes taking place during the crystallizing and melting processes were investigated for Br^- and I^- salts. Two stable rotational isomers, **Asym** and **Sym**, were revealed by using Raman spectroscopy techniques and DFT calculations. In the liquid states of both salts, **Asym** and **Sym** were found to coexist, with **Asym** dominant at an **Asym/Sym** ratio of about 7/3. Only **Asym** was observed for the most part in crystalline states, although **Sym** is slightly more stable than **Asym** from the standpoint of enthalpy. This is attributed to the entropy effect, conformational multiplicity in particular.

Conformational changes of [*i*-C_3mim]$^+$ during the crystallizing and melting processes are directly observed by conducting simultaneous measurements using Raman spectroscopy and calorimetry techniques. As for the crystallizing process, conformational changes from **Sym** to **Asym** are observed to occur instantaneously. In contrast, during the melting process, conformational changes from **Asym** to **Sym** occur gradually with linking to melting, which causes the premelting phenomenon over a wide temperature range. This observation gives us clear insight into the premelting of ILs and demonstrates the conformational changes between isomers during the crystallizing and melting processes.

Acknowledgment. The present study was supported by a Grant-in-Aid for Scientific Research (No. 17073002) in Priority Area "Science of Ionic Liquids" (Area Number 452) from the Ministry of Education, Culture, Sports, Science and Technology. The authors would like to thank Dr. Tomohiro Mukai for his useful advice in synthesis of the samples.

Supporting Information Available: Tables listing atom coordinates and vibratinonal frequencies for both **Asym** and **Sym** cacluated at the B3LYP/6-311+G(d,p) level of theory. This material is available free of charge via the Internet at http://pubs.acs.org.

References and Notes

(1) *Ionic Liquids in Syntheses*; Wasserscheid, P., Welton, T. Eds.; VCH-Wiley: Weinheim, Germany, 2003.
(2) *Electrochemical Aspects of Ionic Liquids*; Ohno, H. Ed.; Wiley-Interscience: Hoboken, NJ, 2005.
(3) Welton, T. *Chem. Rev.* **1999**, *99*, 2071–2083.
(4) Wasserscheid, P.; Keim, W. *Angew. Chem., Int. Ed.* **2000**, *39*, 3772–3789.
(5) Sheldon, R. *Chem. Commun.* **2001**, 2399–2407.

(6) Dzyuba, S. V.; Bartsch, R. A. *ChemPhysChem* **2002**, *3*, 161–166.
(7) Paulechka, Y. U.; Kabo, G. J.; Blokhin, A. V.; Shaplov, A. S.; Lozinskaya, E. I.; Vygodskii, Ya. S. *J. Chem. Thermodyn.* **2007**, *39*, 158–166.
(8) Holbrey, J. D.; Reichert, W. M.; Nieuwenhuyzen, M.; Johnston, S.; Seddon, K. R.; Rogers, R. D. *Chem. Commun.* **2003**, 1636–1637.
(9) Holbrey, J. D.; Seddon, K. R. *J. Chem. Soc., Dalton Trans.* **1999**, 2133–2139.
(10) Fox, D. M.; Awad, W. H.; Gilman, J. W.; Maupin, P. H.; DeLong, H. C.; Trulove, P. C. *Green Chem.* **2003**, *5*, 724–727.
(11) Ngo, H. L.; LeCompte, K.; Hargens, L.; McEwen, A. B. *Thermochim. Acta* **2000**, *357*, 97–102.
(12) Nishikawa, K.; Wang, S.; Katayanagi, H.; Hayashi, S.; Hamaguchi, H.; Koga, Y.; Tozaki, K. *J. Phys. Chem. B* **2007**, *111*, 4894–4900.
(13) Endo, T.; Tozaki, K.; Masaki, T.; Nishikawa, K. *Jpn. J. Appl. Phys.* **2008**, *47*, 1775–1779.
(14) Umebayashi, Y.; Fujimori, T.; Sukizaki, T.; Asada, M.; Fujii, K.; Kanzaki, R.; Ishiguro, S. *J. Phys. Chem. A* **2005**, *109*, 8976–8982.
(15) Frisch, M. J.; Trucks, G. W.; Schlegel, H. B.; Scuseria, G. E.; Robb, M. A.; Cheeseman, J. R.; Montgomery, J. A., Jr.; Vreven, T.; Kudin, K. N.; Burant, J. C.; Millam, J. M.; Iyengar, S. S.; Tomasi, J.; Barone, V.; Mennucci, B.; Cossi, M.; Scalmani, G.; Rega, N.; Petersson, G. A.; Nakatsuji, H.; Hada, M.; Ehara, M.; Toyota, K.; Fukuda, R.; Hasegawa, J.; Ishida, M.; Nakajima, T.; Honda, Y.; Kitao, O.; Nakai, H.; Klene, M.; Li, X.; Knox, J. E.; Hratchian, H. P.; Cross, J. B.; Adamo, C.; Jaramillo, J.; Gomperts, R.; Stratmann, R. E.; Yazyev, O.; Austin, A. J.; Cammi, R.; Pomelli, C.; Ochterski, J. W.; Ayala, P. Y.; Morokuma, K.; Voth, G. A.; Salvador, P.; Dannenberg, J. J.; Zakrzewski, V. G.; Dapprich, S.; Daniels, A. D.; Strain, M. C.; Farkas, O.; Malick, D. K.; Rabuck, A. D.; Raghavachari, K.; Foresman, J. B.; Ortiz, J. V.; Cui, Q.; Baboul, A. G.; Clifford, S.; Cioslowski, J.; Stefanov, B. B.; Liu, G.; Liashenko, A.; Piskorz, P.; Komaromi, I.; Martin, R. L.; Fox, D. J.; Keith, T.; Al-Laham, M. A.; Peng, C. Y.; Nanayakkara, A.; Challacombe, M.; Gill, P. M. W.; Johnson, B.; Chen, W.; Wong, M. W.; Gonzalez, C.; Pople, J. A. *Gaussian 03*; Gaussian, Inc.: Wallingford, CT, 2004.
(16) Becke, A. D. *J. Chem. Phys.* **1993**, *98*, 5648–5652.
(17) Lee, C.; Yang, W.; Parr, R. G. *Phys. Rev. B* **1988**, *37*, 785–789.
(18) Miehlich, B.; Savin, A.; Stoll, H.; Preuss, H. *Chem. Phys. Lett.* **1989**, *157*, 200–206.
(19) Turner, E. A.; Pye, C. C.; Singer, R. D. *J. Phys. Chem. A* **2003**, *107*, 2277–2288.
(20) Kawahata, M.; Endo, T.; Yamaguchi, K.; Seki, H.; Nishikawa, K. In preparation.
(21) Golovanov, D. G.; Lyssenko, K. A.; Vygodskii, Ya. S.; Lozinskaya, E. I.; Shaplov, A. S.; Antipin, M. Yu. *Russ. Chem. Bull., Int. Ed.* **2006**, *55*, 1989–1999.
(22) Fujimoto, T.; Kawahata, M.; Nakakoshi, M.; Machinami, T.; Seki, H.; Tashiro, M. *Anal. Sci.* **2007**, *23*, x223–x224.
(23) Ozawa, R.; Hayashi, S.; Saha, S.; Kobayashi, A.; Hamaguchi, H. *Chem. Lett.* **2003**, *32*, 948–949.
(24) Hayashi, S.; Ozawa, R.; Hamaguchi, H. *Chem. Lett.* **2003**, *32*, 498–499.
(25) Berg, R. W.; Deetlefs, M.; Seddon, K. R.; Shim, I.; Thompson, J. M. *J. Phys. Chem. B* **2005**, *109*, 19018–19025.
(26) Fujii, K.; Fujimori, T.; Takamuku, T.; Kanzaki, R.; Umebayashi, Y.; Ishiguro, S. *J. Phys. Chem. B* **2006**, *110*, 8179–8183.
(27) Lassègues, J. C.; Grondin, J.; Holomb, R.; Johansson, P. *J. Raman Spectrosc.* **2007**, *38*, 551–558.
(28) Berg, R. W. *Monatsh. Chem.* **2007**, *138*, 1045–1075.

JP8031989